Adsorption (2013) 19:1245–1252
DOI 10.1007/s10450-013-9565-9

GCMC simulation of argon adsorption in wedge shaped mesopores of finite length

Zahra Nickmand · D. D. Do · D. Nicholson · Seyed Foad Aghamiri · Mohammad Reza Talaie Khozanie · Hasan Sabzyan

Received: 3 April 2013 / Accepted: 5 August 2013 / Published online: 13 August 2013

Abstract We have used Grand Canonical Monte Carlo simulation to study argon adsorption at 87 K in wedge shaped mesopores. The structural parameters, including mean pore size, wall length and wedge angle, were varied to investigate their effects on the size, shape and the position of the hysteresis loop. Although the effects of pore size have been studied previously, the wall length and wedge angle have received little attention. We find that the wedge angle can have a significant effect on the existence, position, size and shape of the hysteresis loop, while the wall length affects the adsorptive capacity associated with the loop and the behaviour of the isotherm beyond the loop. The results of this work have far-reaching consequences for the characterization of pore size distribution where it is commonly assumed, when constructing a kernel of local isotherms, that pore size is uniform, since even a small deviation from a constant pore width can shift the condensation and evaporation pressures significantly and thus lead to an incorrect estimation of pore size.

Keywords Adsorption · Characterization · Hysteresis · Slit mesopore · Wedge mesopore

Z. Nickmand · D. D. Do (✉) · D. Nicholson
School of Chemical Engineering, University of Queensland, St. Lucia, QLD 4072, Australia
e-mail: d.d.do@uq.edu.au

Present Address:
Z. Nickmand · S. F. Aghamiri · M. R. T. Khozanie
Department of Chemical Engineering, University of Isfahan, 81746-73441 Esfahan, Iran

Present Address:
H. Sabzyan
Department of Chemistry, University of Isfahan, 81746-73441 Esfahan, Iran

1 Introduction

Mesoporous materials such as silica gel, alumina and carbon are widely used in industry as adsorbents for separation and purification and as supports for dispersing active agents for catalytic chemical reaction. For optimal utilization of porous solids in specific applications, porous solids must be characterized for surface chemistry and structural properties, such as surface area, pore size and pore volume (Thommes 2004). For mesoporous solids, surface area can be reliably determined with the classical BET method, although DFT and Grand Canonical Monte Carlo (GCMC) tools have been increasingly used as a better alternative in obtaining more meaningful geometrical surface area because the BET-area could be affected by the pressure range over which the area is determined. More often than not, the area determined by the BET method is greater than the geometrical area determined using GCMC simulation (Do and Do 2005). To determine pore size and volume, one has to carry out adsorption measurements under conditions where the pores fill with liquid condensate. Simple gases such as nitrogen and argon at their respective boiling points, fill mesopores at pressures below saturation vapour pressure. The amount required to fill the pores is used to determine the mesopore volume while the pressures at which the condensation and evaporation occur are used to determine the distribution of pore size (Gregg and Sing 1982). Usually, condensation and evaporation in mesoporous solids occur over different ranges of pressure, and the size, shape and position of the hysteresis loop for a single isolated pore are strongly affected by its topology and its structural properties, such as pore size and length. Pore topology includes a number of properties such as curvature of the pore (slit, cylinder or sphere), non-uniformity of the pore cross section, including geometric corrugation,

variation in adsorbent energy along the pore, whether pore ends are open or closed to the surroundings, or the pore is in the form of a cavity connected to the surrounding via narrower necks, etc. Much research has been carried out to establish the relationship between the shape of the hysteresis loop and the pore topology. The first step in this direction is to classify the shape of the hysteresis loop (Sing et al. 1985; Thommes 2004; Nguyen et al. 2011). de Boer (de Boer 1958; Sing et al. 1985; Thommes 2004) was the first to propose a classification hysteresis loops. He identified five types, which he labeled A–E. A decade later the IUPAC published a new classification comprising four types, labeled H1–H4. Notably Type C in the de Boer classification, was omitted from the IUPAC classification. de Boer associated this type of loop with cavities that could be emptied through windows with a wide range of window openings, so that each cavity would be emptied when its window became sub critical; the implicit assumption being that each window has a direct pathway to the external adsorptive phase. Figure 1a, b illustrate the hysteresis loops, as classified by de Boer and by the IUPAC, that are relevant to the discussion in this paper.

With the advance in the synthesis of new materials, especially ordered mesoporous solids, and the advance in modern theoretical tools, notably the DFT and GCMC methods, many publications have appeared adding to our better understanding of how pore condensation and evaporation occur. Since pore structure can now be tailored in some cases, theoretical studies have been carried out to understand the various aspects of the pore structure

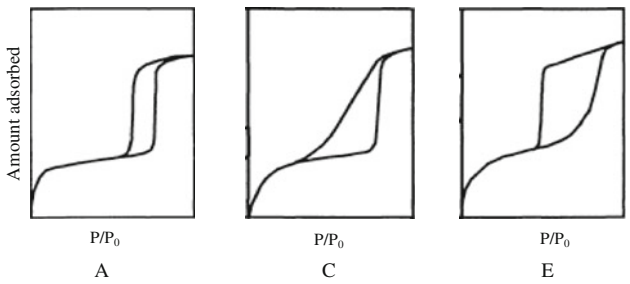

(a) Types A, C and E in de Boer classification

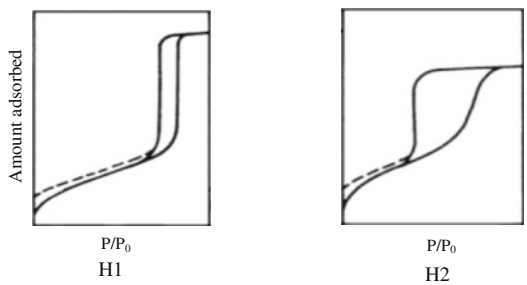

(b) Types H1 and H2 in IUPAC classification

Fig. 1 Various types of hysteresis loop

separately; for example pores with both ends opened or with one end opened (Sarkisov and Monson 2001; Fan et al. 2011). In an early study of the effects of closing pore ends Papadopoulou et al. (1992) used both the grand canonical and canonical ensembles to study adsorption of simple gases in cylindrical and slit-like pores, and found that the adsorption branch is not affected by the pore length, compared to the corresponding pore of infinite length (modeled with periodic boundary conditions), while the desorption branch was strongly affected because of the presence of the menisci starting from the ends in pores with open ends. The effects of closing one end were studied by Sarkisov and Monson (2001) who used both molecular dynamics and GCMC simulations, and found that hysteresis was absent in pores with a closed end but was present in the corresponding pore with both ends exposed to the surroundings. Vanin and Brodskaya (2011) investigated the adsorption isotherms of methane in a graphitic wedge shaped pore by GCMC and the multiple histogram reweighting method. They studied the behaviour of adsorption at different temperatures and for different wedge angles. The effects of a closed end ink bottle structure on adsorption in a finite slit-like pore were recently studied by Fan et al. (2011); who showed that both pore width and pore length have a significant effect on the size and the location of the hysteresis loop. Nguyen et al. (2013) found that the hysteresis loop for cylindrical pores with non-uniform size and corrugation decreases and shifts to lower pressure with decrease in pore width, and most importantly the loop shape changes from Type H1 (according to the IUPAC classification) to Type C in de Boer classification.

Here we have extended this earlier work to examine more fully the effects of pore width, length and wedge angle in wedge-shaped pores, on the adsorption–desorption hysteresis of argon at 87 K. The hysteresis loops exhibit a quite remarkable range of patterns in response to changes in these geometrical factors; a significant result is that we find that loops that are closely similar to the de Boer Type C pattern can often occur for this type of geometry. Our work deals exclusively with wedges that have two ends open to the bulk surroundings. For a wedge with its apex closed, readers should refer to seminal work by Rascon and Parry (2005).

2 Theory

2.1 Slit pore model

The GCMC method (Frenkel and Smit 2002) was used to simulate argon adsorption in a wedge shaped pore with walls comprised of three graphene layers. A schematic diagram of a wedge pore and the structural parameters

defining its geometry: pore size (H), wall length (L) and wedge angle (α), are shown in Fig. 2. The wall length along the wedge direction (y-direction) was finite and periodic boundaries were applied in the x-direction. The two ends of the wedge were open to the surroundings, and the mean pore size is defined as:

$$H_m = \frac{H_1 + H_2}{2} \quad (1)$$

where H_1 and H_2 are the pore widths at the two ends. When the wedge angle is zero, we recover a slit pore with uniform pore width, which will be used as a reference for comparison.

2.2 Potential model and simulation details

The intermolecular interaction energy of argon was modeled with the 12-6 Lennard-Jones equation (Prausnitz et al. 1998) and the solid–fluid interaction energy was calculated with the Bojan–Steele equation (Bojan and Steele 1988), with the cross molecular parameters, ε_{sf} and σ_{sf}, calculated from the Lorentz-Berthelot combining rules. The relevant molecular parameters are listed in Table 1.

In the GCMC simulations we used 2×10^4 cycles for equilibration and sampling stages, with at least 2,000 moves in each cycle. We chose displacement, insertion and deletion trials with probabilities of 0.2, 0.4 and 0.4, respectively, and a cut-off radius of five times the collision diameter of argon. The equation of state of Johnson et al. (1993) was used to relate the chemical potential to the bulk gas pressure.

The overall pore density is defined as (Do and Do 2007):

$$\rho = \frac{\langle N \rangle - \rho_{gas} V_{acc}}{V_{acc}} \quad (2)$$

where ρ_{gas} is the bulk molecular density, $\langle N \rangle$ is the average number of molecules in the pore region, and V_{acc} is the accessible pore volume which is defined as one in which the solid–fluid potential is negative.

To better understand the adsorption–desorption mechanisms, we calculate the mesoscopic density from the two-dimensional (2D) bin density. To obtain the latter, we divide the pore space into bins in the y- and z-directions as shown in Fig. 3, and calculate the 2D-local density of the bin (i,j) as follows:

$$\rho = N_{ij}/V_{ij} \quad (3)$$

where N_{ij} is the number of molecules in the bin and V_{ij} is its volume. The mesoscopic density at the bin (i,j) is calculated by summing the molecules falling within a radius R around the bin (i,j) and dividing by their total volume. In this work we used a bin size of 0.1σ and $R = 0.5\sigma$.

Table 1 The LJ potential parameters of argon and solid atom used in this study

i	σ_{ii} (Å)	ε_{ii}/k (K)	Ref.
Fluid (argon)	3.405	119.8	Michels et al. (1949)
Solid atom (carbon)	3.4	28	Steele (1974)

3 Results and discussion

First we present results for argon adsorption in a slit pore of uniform size to examine the effects of pore size and length and to establish a reference for comparison with the wedge shaped pores.

3.1 Slit pore of uniform pore width

Adsorption and desorption isotherms for slit pores of uniform width have been studied using GCMC simulation (Fan et al. 2011). In the micropore region, the mechanism is pore-filling and the isotherm is reversible. When the pore width exceeds a *critical* value at a given pore length, a hysteresis loop appears. The loop area increases and shifts to higher pressures with increasing pore-size. This implies that there is a threshold pore size above which there are only adsorbed layers in the pore until pressure has reached the saturation vapor pressure when the liquid adsorbate condenses. This is a consequence of the finite length of the pore, and this threshold width increases with pore length. Figure 4, summarizes these limits in the form of a parametric map showing the width and length

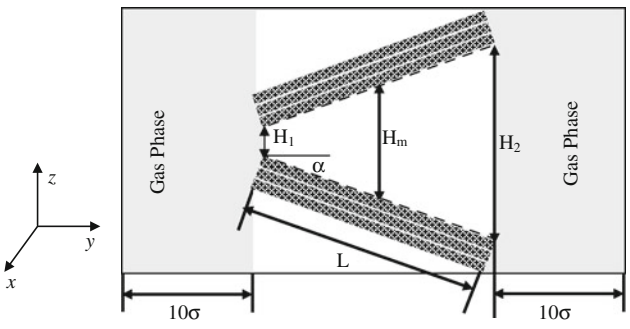

Fig. 2 Configuration of wedge shaped pore

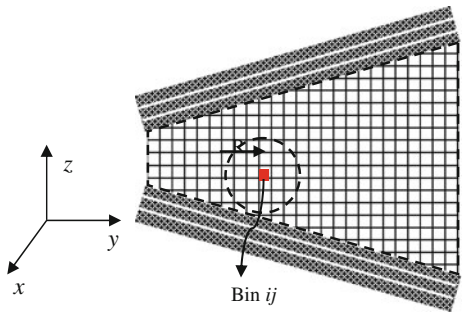

Fig. 3 Division of the wedge shaped pore into square bins in the y and z directions

regions in which hysteresis occurs. The solid line is the critical hysteresis pore size as a function of wall length, and the dashed line is the threshold pore width above which there is no pore condensation. For example for the pore of length 4 nm, the isotherms are reversible for pore sizes less than 1.9 nm as expected for micropores. When the pore size is greater than 1.9 nm, a hysteresis loop appears and its area increases with pore width until this reaches 4.5 nm; above this, there is no condensation below the saturation vapor pressure. The inset of Fig. 4 shows the isotherms for these pores.

In Fig. 5 we have plotted the relative pressure for condensation and evaporation as a function of pore width for pores of 6 nm length; the critical pore width is 1.8 nm and the threshold pore width is 5 nm (derived from Fig. 4). As seen in Fig. 5, the loop size, measured as the vertical distance between the two branches, increases as pore size increases from 1.8 to 5 nm.

3.2 Wedge shaped pores

Figure 6 shows adsorption isotherms for wedge pores of length 6 nm having different wedge angles and an average pore size of 5 nm. We define the following abbreviations to indicate which process is operating along the isotherm: where L is the build up of molecular layers, C is the condensation, M_a is the advance of meniscus to the pore mouth, M_d is the withdrawal of meniscus to the pore interior, E is the evaporation, R is the thinning of molecular layers

The figure shows that wedge angle has a significant effect on the isotherm. As the angle is increased, we observe the following:

1. The loop area decreases, its position shifts to lower pressures, and the loop finally disappears at a critical angle.

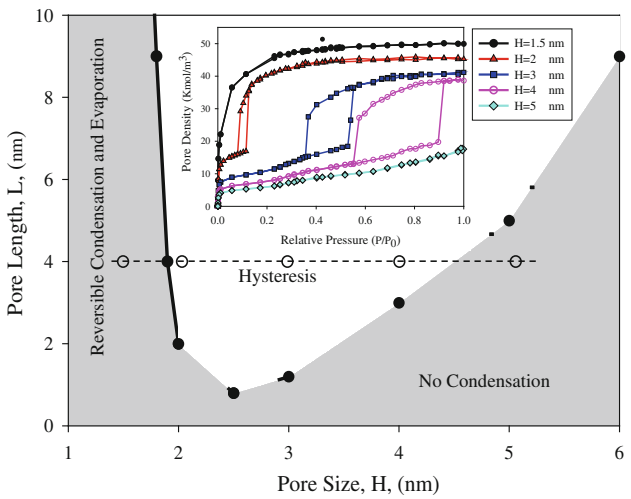

Fig. 4 Parametric map of argon adsorption in a slit pore of uniform width at 87 K. The *inset* shows isotherms for pores of length 4 nm

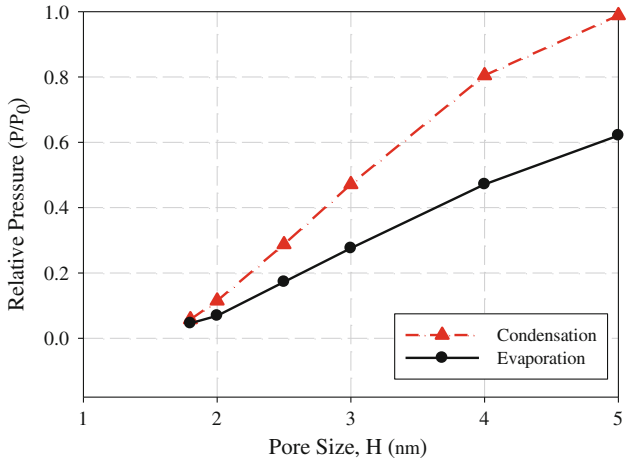

Fig. 5 Relative pressures for condensation and evaporation of argon at 87 K in slit pores of uniform width and 6 nm length

2. The loading prior to condensation decreases and the loading for adsorption after condensation increases.
3. As the wedge angle is increased from 0° to 5°, the ratio of the adsorption capacity at evaporation (E) to that at the withdrawal of the meniscus (M_d), increases resulting in a change of the hysteresis loop type from C to H1. However, when the angle is increased from 5° to 30°, this ratio decreases again and the loop reverts to Type C, and diminishes in size (point 1). As the angle is increased further, the loop disappears as the wedge pore approximates to two independent flat surfaces.

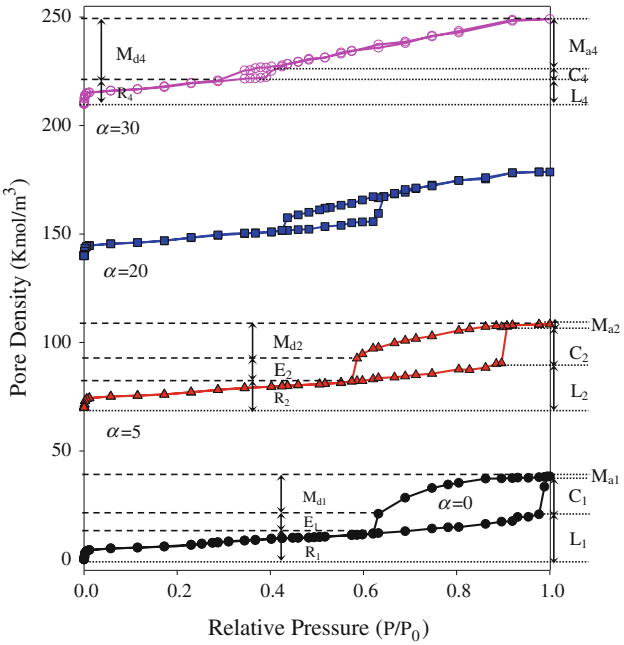

Fig. 6 Isotherms for argon adsorption at 87 K in a wedge-shaped pore of length 6 nm and mean pore size of 5 nm. The wedge angles are 0°, 5°, 20° and 30°. The isotherms for wedge angles 5°, 20° and 30° have been shifted up by 70, 140 and 210 kmol/m^3, respectively

To explain these observations in greater detail, we examine adsorbate density distributions just before and just after condensation and evaporation. Examples of these are shown in Figs. 7 and 8 for a slit pore of uniform width 5 nm and a wedge-shaped pore of mean pore width 5 nm and wedge angle 20°.

In the uniform slit pore, adsorption follows a molecular layering mechanism and the adsorbed layers associated with the two pore walls bulge with an increase in pressure until the pressure has reached the condensation pressure when a liquid bridge is formed which then extends along the pore width and forms two hemi-cylindrical menisci at the pore ends (Fig. 7). The pore completely fills as pressure approaches P_0, where the menisci become flat. On desorption, menisci are formed at the pore mouths and recede into the pore interior as pressure is decreased. Close to the evaporation pressure, the liquid bridge is a bi-concave liquid lens that breaks at the evaporation at the evaporation pressure. It is now well-established (Fan et al. 2011) that the adsorbate in slit-shaped mesopores is in the form of convex adsorbed layers just before condensation and a bi-concave liquid bridge just before evaporation. Not only are the curvatures different in adsorption and desorption, their isotherms are metastable prior to condensation and evaporation and the equilibrium transition falls somewhere between the adsorption and desorption boundaries of the hysteresis loop.

In wedge-shaped pores, adsorption begins as molecular layering, in the same way as in uniform slit pores, but the layers are thicker at the narrower end where the greater overlap of the solid–fluid potential from the opposing walls deepens the potential well, as illustrated by the density profiles in Fig. 8. Since the adsorbed layer is thicker at the narrower end, this is where a liquid bridge is first formed when the condensation pressure is reached. In contrast to the uniform pore, the liquid bridge does not extend over the full length of the pore, and the curvature of the meniscus at the narrower end is lower than that of the uniform slit pore, while the curvature of the meniscus at the wider end is greater.

When the wedge angle is increased while keeping the mean pore width and pore length constant, we observe the following:

1. Condensation occurs at a lower pressure, and the liquid bridge is smaller in size and more localized towards the narrower end where the solid–fluid interactions are stronger and consequently the adsorbed amount at condensation is smaller. The evaporation pressure is also lower on desorption and the amount of adsorbate retained at evaporation is also smaller.
2. The curvature of the meniscus at the narrower end is greater than that at the wider end.
3. After condensation the meniscus advances towards the wider end, and the amount adsorbed during this process increases with the wedge angle; while on desorption the process before the evaporation of the liquid bridge is

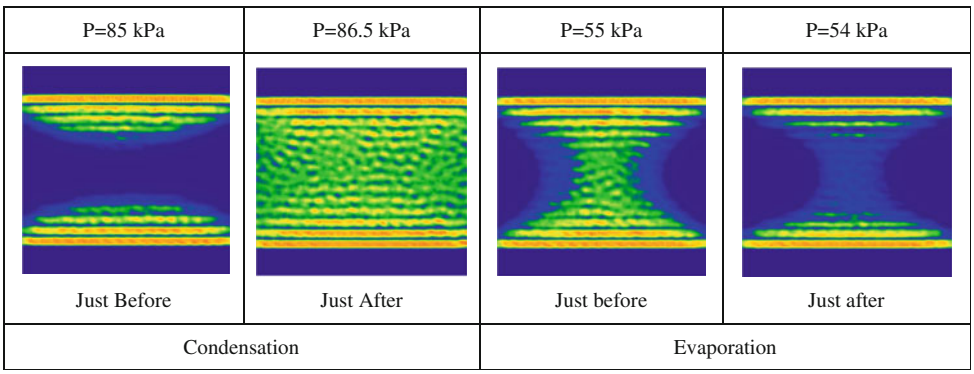

Fig. 7 Density distributions of argon adsorption at 87 K in a uniform slit pore of width 5 nm and length 6 nm

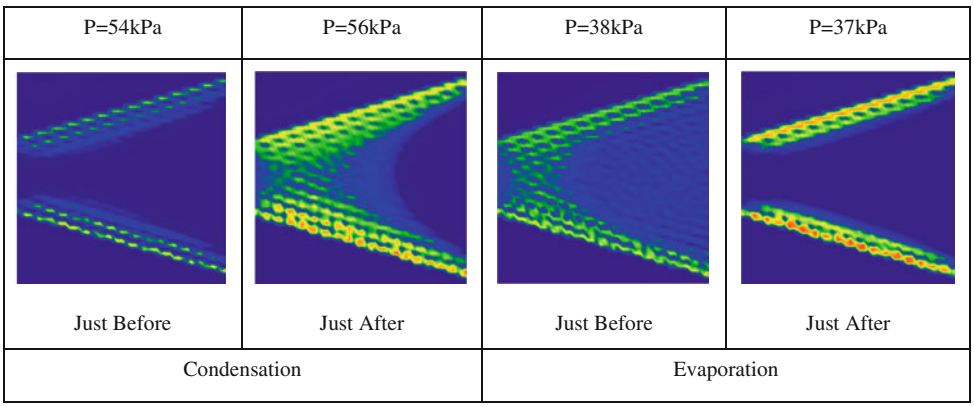

Fig. 8 Density distributions of argon adsorption at 87 K in the wedge-shaped pore with mean pore width of 5 nm and a wedge angle of 20°

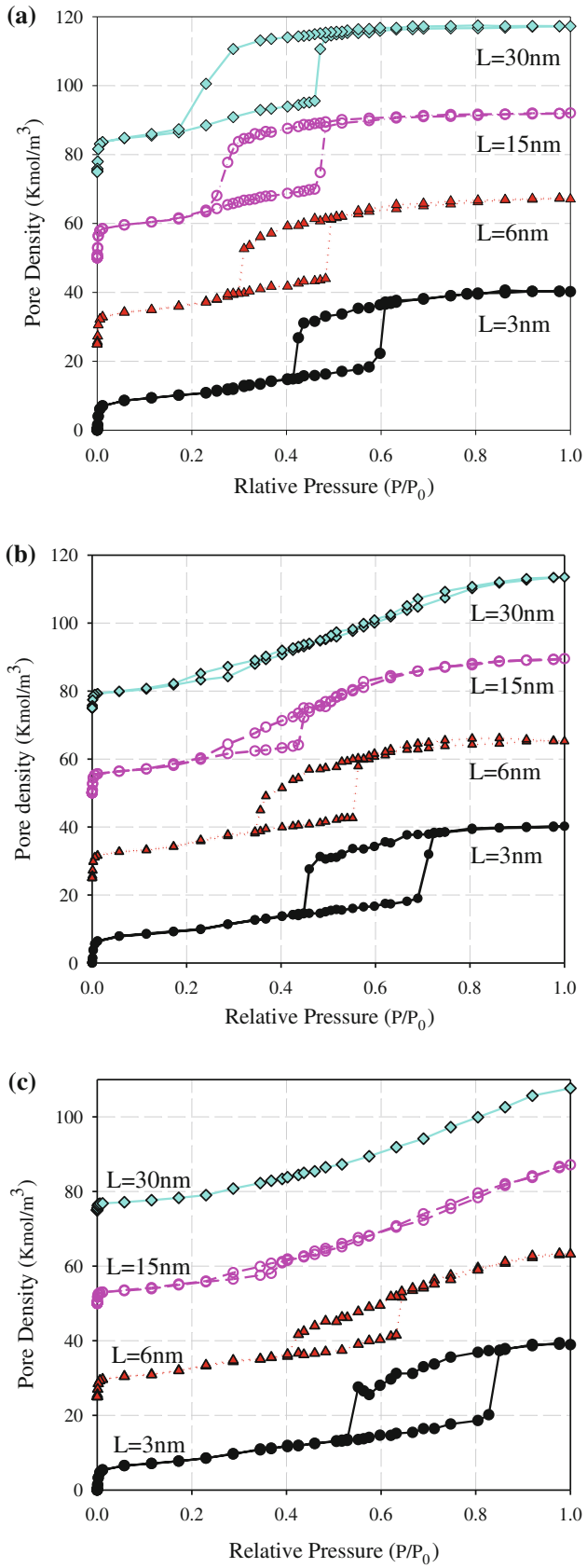

◀**Fig. 9** Adsorption isotherms for argon at 87 K in **a** a slit pore with uniform pore width 3 nm, **b** a wedge shaped pore with a wedge angle of 5° narrower end width 3 nm and **c** wedge shaped pore with a wedge angle of 20° narrower end width 3 nm for lengths of 3, 6, 15, and 30 nm. The isotherms for pores having lengths of 6, 15, and 30 nm have been shifted up by 25, 50, and 75 kmol/m^3, respectively

withdrawal of the menisci, mostly contributed by the meniscus at the wider end.

Both the wedge angle and the pore length affect the isotherm, the effects of pore length are particularly interesting.

Figure 9a shows isotherms for uniform 3 nm slits of lengths: 3, 6, 15 and 30 nm. As the length is increased, the onset of the hysteresis loop shifts to lower pressures and reaches a limiting pressure when the length is greater than 30 nm (L/H = 10). As the pore length increases, the loop type moves from H1 towards Type C, a feature which does not seem to have been recognized previously.

Figure 9b, c show isotherms for wedge pores narrow end widths of 3 nm and lengths of 3, 6, 15 and 30 nm. As the wall length is increased the following may be observed:

1. The hysteresis loop shifts to lower pressures.
2. The hysteresis loop changes from Type H1 to Type C.
3. The area of the hysteresis loop decreases and the loop disappears for lengths greater than 30 nm.

Except for point (3), hysteresis in the wedge-shaped pore follows a similar pattern to that in the uniform size pore.

In Fig. 10a, b we show the density distributions along the pore length for the uniform slit of 3 nm width and for a wedge-shaped with a width at the narrow end of 3 nm and wedge angle of 20° at relative pressures, below the condensation pressure, of 0.46 and 0.37, respectively.

In the parallel sided pore (Fig. 10a), the distributions are the same for pores having 6 and 15 nm lengths. In the short pore of 3 nm length, the solid–fluid interaction is weaker, and consequently there are fewer molecules in the centre of the pore and condensation in this pore occurs at a higher pressure. In the longer pores the number of molecules in the centre of the pore is the same, resulting in the same condensation pressures (c.f. Fig. 9a).

In the wedge-shaped pores the condensation and evaporation pressures decrease continuously when the wall length is increased, and the loop disappears in pores longer than 30 nm, which is distinctly different from the uniform pores. Figure 10b confirms the mechanism already described, where condensation at the narrower end at a lower pressure, creates a smaller liquid bridge and this is followed by the advance of the meniscus towards the larger end. The amount adsorbed in the second process is increasingly greater than that in the initial condensation as the wall

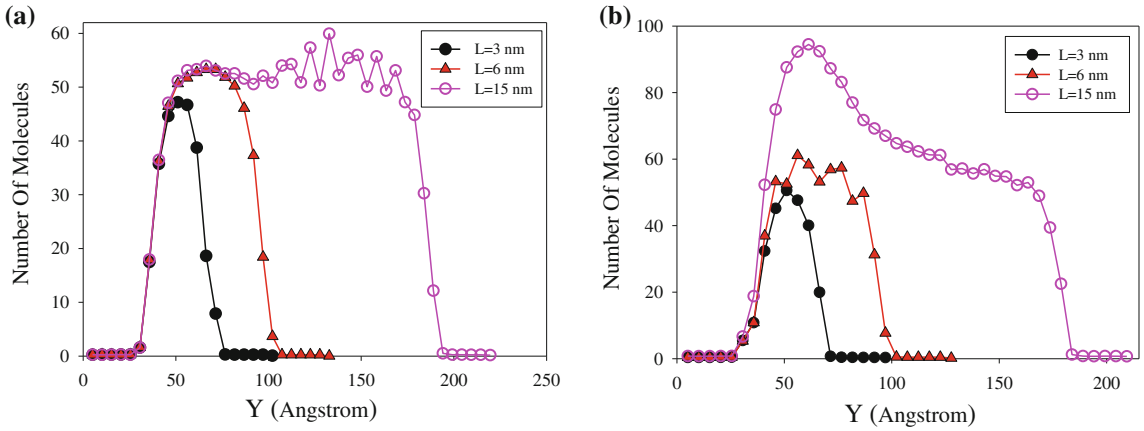

Fig. 10 Local density distributions of argon adsorbed at 87 K in **a** the uniform slit pore of width 3 nm at relative pressure of 0.46 and **b** a wedge-shaped pore with a wedge angle of 20° narrower end of 3 nm width at relative pressure of 0.37

length is increased, and since the movement of the meniscus is reversible, the adsorption isotherm is also reversible because of the small contribution made by condensation.

4 Conclusion

We have investigated argon adsorption at 87 K in finite wedge-shaped slit pores and in a uniform slit pore using GCMC simulation. In the uniform slit pore with pore widths ranging from 1.5 to 6 nm the critical length above which hysteresis occurs was determined. From our extensive simulation, we have plotted a parametric map of pore length versus pore width: at a given pore length, we find that there is a critical pore width above which hysteresis exists and a threshold pore width above which there is no condensation in the pore below the saturation pressure.

For wedge-shaped pores, both the angle and the pore length have a significant effect on the hysteresis loop. Even for pores with small wedge angles, the area and shape of the hysteresis loop is significantly different from that for the corresponding uniform pores. Specifically, the condensation and evaporation pressures are different from those in uniform pores, and this suggests that a kernel of local isotherms based on uniform pore widths might lead to significant error in the determination of pore size distributions in nanoporous materials which have this type of structure.

Acknowledgement We would like to thank the Ministry of Research Science and Technology of Iran for financial support. This project is also supported by the Australian Research Council.

Appendix

See Fig. 11.

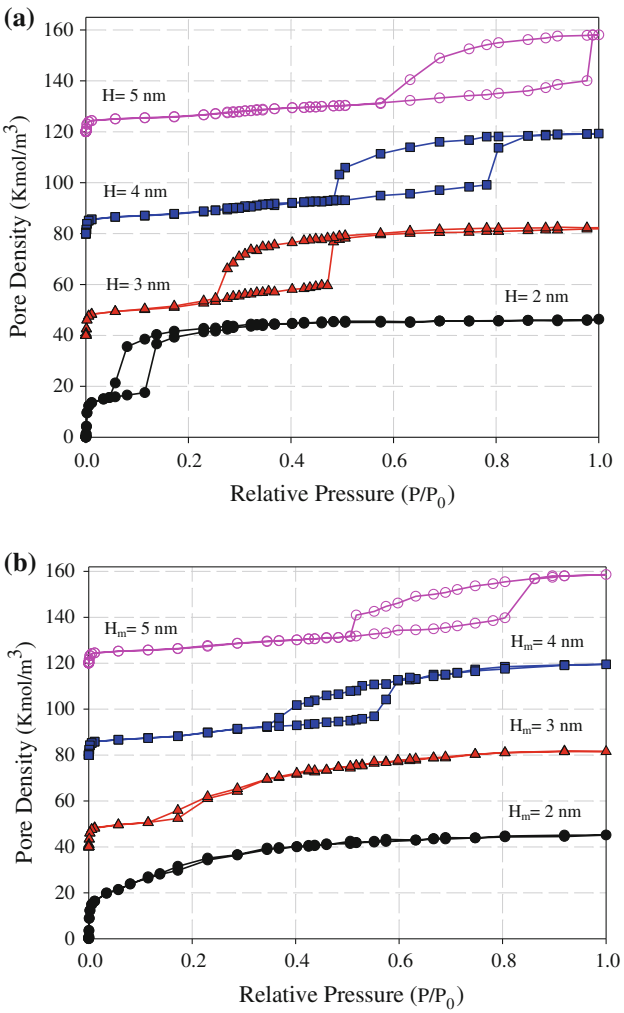

Fig. 11 The effect of pore size on adsorption of argon in the **a** slit pore with uniform pore width and length of 6 nm and **b** wedge shaped pore with a wedge angle of 10° and wall length of 6 nm. The isotherms for pore sizes of 3, 4 and 5 nm have been shifted up by 35, 70, 75 and 105 kmol/m^3, respectively

References

Bojan, M.J., Steele, W.A.: Computer simulation of physisorption on a heterogeneous surface. Surf. Sci. **199**(3), L395–L402 (1988)

de Boer, J.H.: The structure and properties of porous materials. Colston Papers Butterworths, London (1958)

Do, D.D., Do, H.D.: Adsorption of argon on homogeneous graphitized thermal carbon black and heterogeneous carbon surface. J. Colloid Interface Sci. **287**(2), 452–460 (2005)

Do, D.D., Do, H.D.: Appropriate volumes for adsorption isotherm studies: The absolute void volume, accessible pore volume and enclosing particle volume. J. Colloid Interface Sci. **316**(2), 317–330 (2007)

Fan, C.Y., Do, D.D., Nicholson, D.: On the cavitation and pore blocking in slit-shaped ink-bottle pores. Langmuir **27**(7), 3511–3526 (2011)

Frenkel, D., Smit, B.: Understanding molecular simulation: from algorithms to applications. Academic Press, San Diego (2002)

Gregg, S.J., Sing, K.S.W.: Adsorption, surface area and porosity. Academic Press, London (1982)

Johnson, J.K., Zollweg, J.A., Gubbins, K.E.: The Lennard-Jones equation of state revisited. Mol. Phys. **78**(3), 591–618 (1993)

Michels, A., Wijker, H., Wijker, H.: Isotherms of argon between 0 °C and 150 °C and pressures up to 2900 atmospheres. Physica **15**(7), 627–633 (1949)

Nguyen, P.T.M., Do, D.D., Nicholson, D.: On the hysteresis loop of argon adsorption in cylindrical pores. J. Phys. Chem. C **115**(11), 4706–4720 (2011)

Nguyen, P.T.M., Do, D.D., Nicholson, D.: Simulation study of hysteresis of argon adsorption in a conical pore and a constricted cylindrical pore. J. Colloid Interface Sci. **396**, 242–250 (2013)

Papadopoulou, A., Swol, F.V., Marconi, U.M.B.: Pore-end effects on adsorption hysteresis in cylindrical and slit like pores. J. Chem. Phys. **97**(9), 6942–6952 (1992)

Rascon, C., Parry, A.O.: Covariance for cone and wedge complete filling. Phys. Rev. Lett. **94**, 096103 (2005)

Prausnitz, J., Lichtenthaler, R., de Azevedo, E.: Molecular thermodynamics of fluid-phase equilibria, 3rd edn. Prentice Hall, New Jersey (1998)

Sarkisov, L., Monson, P.A.: Modeling of adsorption and desorption in pores of simple geometry using molecular dynamics. Langmuir **17**(24), 7600–7604 (2001)

Sing, K.S.W., Everett, D.H., Haul, R.A.W., Moscou, L., Pierotti, R.A., Rouquerol, J., Siemieniewska, T.: Reporting physisorption data for gas/solid systems with special reference to the determination of surface area and porosity (Recommendations 1984). Pure Appl. Chem. **57**(4), 603–619 (1985)

Steele, W.A.: The interaction of gases with solid surfaces. Pergamon Press, Oxford (1974)

Thommes, M.: Physical adsorption characterization of ordered and amorphous mesoporous materials. In: Lu, G., Zhao, X.S. (eds.) Nanoporous Materials, Science & Engineering, vol. 4, pp. 317–364. Imperial College Press, New Jersey (2004)

Vanin, A.A., Brodskaya, E.N.: Computer simulation of Lennard-Jones fluid adsorption in wedge-shaped pores with smooth walls. Colloid J. **73**(4), 445–452 (2011)